NJC

PAPER

View Article Online
View Journal | View Issue

Cite this: *New J. Chem.*, 2021, 45, 2742

Tetranuclear copper(II) cubane complexes derived from self-assembled 1,3-dimethyl-5-(*o*-phenolate-azo)-6-aminouracil: structures, non-covalent interactions and magnetic property†

Nishithendu Bikash Nandi,[a] Atanu Purkayastha,[a] Shaktibrata Roy,[a] Julia Kłak,*[b] Rakesh Ganguly,*[c] Ibon Alkorta *[d] and Tarun Kumar Misra *[a]

Tetranuclear copper(II) complexes are of paramount importance in structural biology, and they are potential materials for magnetism and catalysis. To develop such a system, a new 6-aminoazouracil ligand, 1,3-dimethyl-5-(*o*-phenolate-azo)-6-aminouracil (H_2L, 1) with a N_uN_aO (N_u, uracil-N and N_a, azo-N) chromophore was synthesized and used to generate a noble discrete doubly opened Cu_4O_4 cubane-like cluster ($[CuL]_4{\cdot}2H_2O$, **2.2H$_2$O**) for studying magnetism. The coordination environment of Cu(II) is distorted square planar linked through phenolate-μ_2-O bridges. The ligand crystallizes in the monoclinic space group $P12_1/c1$ and the complex is in the tetragonal $I4_1/a$ space group with an S_4 symmetry. The ligand has two dissociable hydrogen atoms in the solution with pK_1 4.91 (hydrazone proton) and pK_2 9.68 (phenolic proton). In the solid state, the ligand exhibits displaced stacking (energy, −69.5 and −77.3 kJ mol^{-1} for the molecules A and B, respectively) and tetrel bonding interactions (energy, −43.8 kJ mol^{-1}). In **2.2H$_2$O**, the symmetrical units are stacked to show weak noncovalent interactions. The magnetic property of **2.2H$_2$O** was investigated based on the cubane $[Cu_4O_4]$ core and discussed in detail, resulting in the exchange coupling parameter [(J_1 (short Cu···Cu distances) = −110.1(1) cm^{-1}, J_2 (long Cu···Cu distances) = −27.1(2) cm^{-1})] that indicate a strong antiferromagnetic interaction between tetranuclear copper(II) ions through μ-phenolate linkers, which is a result of the interaction of $d_{x^2-y^2}$ orbitals in the square plane. The EPR study is concomitant with the results of magnetism. Thus, it could be a potential material in the field of antiferromagnetic spintronics as well.

Received 24th October 2020,
Accepted 11th January 2021

DOI: 10.1039/d0nj05232a

rsc.li/njc

1. Introduction

The molecule-based magnetic materials are treated as potential materials in various fields, particularly in magnetism. Molecular magnetism,[1] molecular magnets with non-linear optical (NLO) properties,[2] single molecular magnets (SMM, nanoscopic magnet),[3] molecular magnetic sponges (porous frameworks),[4] magneto chiral dichroism (chiral metal center),[5] and crystal engineering,[1d,6] just to mention a few of many applications of magnetic materials, are found in magnetism. These are developed primarily by linking paramagnetic metal centers with linkers, which are mainly organic building blocks. The architecture of these multi-metal centers may be discrete or multidimensional in nature. However, among the various paramagnetic metal centers for metal-clusters, the copper(II) clusters (Cu_n) have been investigated profoundly. Again, the development of tetranuclear copper(II) clusters containing a Cu_4O_4 group with cubane-like structures is of paramount importance because these could be treated as models of metalloenzyme systems.[7] For example, the tetranuclear copper(II) sulfide cluster is one of the active sites of

[a] *Department of Chemistry, National Institute of Technology, Agartala 799046, Tripura, India. E-mail: tkmisra70@yahoo.com/tkmisra.chem@nita.ac.in; Fax: +91-381-2346360; Tel: +91-381-2346630*
[b] *Faculty of Chemistry, University of Wroclaw, Wroclaw 50383, Poland. E-mail: julia.klak@chem.uni.wroc.pl*
[c] *Shiv Nadar University, NH - 91, Tehsil Dadri, Gautam Buddha Nagar, Uttar Pradesh-201314, India. E-mail: rakesh.ganguly@snu.edu.in*
[d] *Instituto de Química Médica, CSIC, Juan de la Cierva, 3, 28006 Madrid, Spain. E-mail: ibon@iqm.csic.es*

† Electronic supplementary information (ESI) available: In addition, there are various information included as supplementary data. The IR spectra are in Fig. S1 for **1** and Fig. S2 for **2.2H$_2$O** and ^{1}H NMR and ^{13}C NMR spectra in Fig. S3 and S4 are for **1**. The Fig. S5 is shown UV-vis spectra in different buffer solution and plot of absorbance *vs.* pH of **1**. The H-bonded network and stacking feature of **1** are shown in Fig. S6 and S7, respectively. The AIM and NCI plot of **1** is projected in Fig. S8. The tautomeric forms of **1** are given in Scheme S1. The Tables S1–S4 include data of **1** for pK_a values, crystallographic bond lengths and angles, and H-bonded parameters, respectively. The Tables S5 and S6 have bond length and angles of **2.2H$_2$O**. The Table S7 has a comparison of Cu_4 cluster of the present study with ref. 24*a*. CCDC 2040369 and 2040370 include the crystallographic supplementary data for **1** and **2.2H$_2$O**. For ESI and crystallographic data in CIF or other electronic format see DOI: 10.1039/d0nj05232a

the nitrous oxide reductase, metalloenzyme, which binds N_2O for reduction in the nitrogen cycle.[8] Synthetically introduced Cu_4 clusters are potent anti-cancer agents,[9] semiconductors, catalysts,[10] and sensors.[11] Moreover, the tetranuclear copper(II) clusters with cubane core–based molecular magnets have been studied extensively. The study of magnetism on such systems reveals that the paramagnetic Cu(II) centers exhibit ferromagnetic to very strong antiferromagnetic coupling interactions.[12] It is noteworthy to mention that, with continuous technology developments, it is impending to get the limits of silicon-based conventional electronics. Thus, the research in spintronics gets impetus recently, and antiferromagnetic materials are considered to be potential spintronic materials.[13]

Uracil, one of the RNA bases, is employed to make numerous derivatives for applications in biology as well as in medicine.[14–17] Uracil-based azo-derivatives and their metal complexes are promising anion sensors.[18] Particularly, azo-derivatives of 1,3-dimethyl-6-aminouracil and their nickel(II) complexes exhibit interesting properties, namely, azo-hydrazone tautomerism, bio-active molecular conversions, non-covalent interactions and anti-microbial activities.[19–22] In addition, polynuclear metal–organic architectures of nickel(II) complexes with multifunctional spacers based on azo-derivatives of 1,3-dimethyl-6-aminouracil have been explored for structural diversity, conductivity and magnetism.[22,23]

In view of the usefulness of Cu(II) cluster compounds and uracil derivatives in diverse areas, we had made a scheme to explore Cu(II)-complexes based on an azo-derivative of 1,3-dimethyl-6-aminouracil as to develop a potential material for biological and material sciences. In the earlier reports, we demonstrated how *p*-substituent (R = H, SO_2NH_2, COOH, or SO_3H) at the phenyl ring attached with the 6-aminouracil through azo-function makes the derived azo-ligand substituent a specific structural motif.[19–23] However, the effect of *o*-substituent at the phenyl ring is yet to be explored. A group at *o*-position of the phenyl ring with capability to bridge metal ions may yield linear or cyclic polymeric structure. In this regard, –OH and –COOH could be the best choice. Colacio and his research group designed an azo-derivative of 6-aminouracil, that is, 1,3-dimethyl-5-(*o*-carboxyphenylazo)-6-aminouracil by placing –COOH as an *o*-substituent and developed Cu(II)-complexes.[24] They isolated one tetrameric Cu(II), quasi-tetrahedral Cu_4 cluster,[24a] where others were monomeric or H-bonded polymeric structures. One noticeable point is that in the Cu_4-cluster,[24a] the four ligands are not equivalent in terms of coordination to Cu(II) ions. The magnetic property of the Cu_4-cluster was investigated. We have thus designed an azo-ligand of 6-aminouracil by incorporating a hydroxyl (–OH) group at the *o*-position of the phenyl ring (Scheme 1) to have a noble Cu(II) cluster with interesting magnetic properties. Phenolic–OH groups at suitable chelate position of a ligand moiety add a flexibility to design polymeric transition-metal clusters because the –OH group can play a dual-legating role, becoming a part of the chelating frame as well as bridging to a metal ion.[25] Herein, we report a structurally and magnetically characterized tetra copper(II) cluster, a Cu_4O_4 cubane-like framework with an anionic deprotonated tridentate ligand, 1,3-dimethyl-5-(*o*-phenolate-azo)-6-aminouracil (H_2L) (Scheme 1). The cluster has some unique features: (i) the cluster is 1 : 1 Cu : L, where all four ligands have identical coordination modes; (ii) tetranuclear double-open 4+2 cubane-like structures (iii) each Cu(II) has distorted square planar geometry with $N_uN_a(\mu\text{-}O)_2$ coordination environment (N_u for uracil-N, N_a for azo-N, and μ-O for bridging phenolate-O); and (iv) strong antiferromagnetic exchange coupling is observed among the Cu(II) ions in the ground state through phenolate linkers.

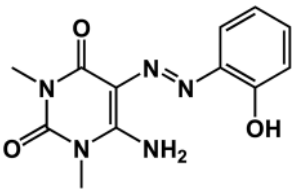

Scheme 1 Molecular structure of 1,3-dimethyl-5-(*o*-phenolate-azo)-6-aminouracil.

2. Experimental

2.1. Materials and instruments

Chemicals including 1,3-dimethyl-6-aminouracil used for the study were of reagent grade. These were having trade mark including Merck, Aldrich, Himedia, and LabChemie and were used without further purification. Solvents were of AR grade, but water was used after double distillation. Standard buffer solutions with varying pH 1–12 were prepared using double-distilled water and chemicals such as HCl, NaOH, $Na_2B_4O_7$, $NaHCO_3$, Na_2CO_3, and KCl. An ionic strength of 0.1 M was maintained with a KCl solution. The pH of the desired buffer solutions were adjusted with either 1 M HCl or 1 M NaOH solution.

A Labtech Digital melting point apparatus was used for melting point determination of the synthesized compounds. A PHM210 standard pH meter (Radiometer, Copenhagen) was used to get accurate pH values of all the buffer solution. IR spectra of KBr pellets of the compounds were recorded using a PerkinElmer, RX-1 FT-IR spectrophotometer in the 4000–400 cm^{-1} region. The ligand in the DMSO-D_6 solvent was run for ^1H and ^{13}C NMR spectra using a JEOL DELTA2 at 500 MHz and 100 MHz, respectively. Absorption spectra of the compounds were studied using a Shimadzu UV-Vis-1800 spectrophotometer. Elemental analyses were conducted using a PerkinElmer 2400 series-II analyzer.

2.2. Synthesis of 1,3-dimethyl-5-(*o*-phenolate-azo)-6-aminouracil: H_2L (1)

The ligand 1,3-dimethyl-5-(*o*-phenolate-azo)-6-aminouracil (H_2L) was synthesized following our reported methods.[19] A solution of *o*-hydroxyphenylamine (0.763 g, 7 mmol) in 6 N HCl (15 mL) was cooled down to 0–5 °C for diazotization using a $NaNO_2$ (7.5 mmol) solution at the same temperature. The diazotized solution was then coupled with 1,3-dimethyl-6-aminouracil (1.08 g, 7 mmol) in an acetic acid–water mixture (2 : 3 v/v) at the same temperature. A very bright yellow solution was developed; the pH of the solution was then adjusted to pH 5–6 for precipitation. The precipitate was filtered off, washed

thoroughly with water and dried in an air oven at 60 °C. For crystallization, a methanolic solution of the product was allowed to evaporate slowly.

Yellow crystal, yield: 75%, m.p. 285 °C, FT-IR (KBr, ν cm^{-1}): 3510–2956 centered at 3290 (O–H, N–H & Ar–H), 1707 & 1619 (^{2}C = 0 & ^{4}C═O), 1531 (C═C), 1476 (N═N), 1256 (C–N), 1074 (C–O str). ^{1}H NMR (DMSO-d$_6$, δ ppm): 11.039 (s,br, ═N–NH), 8.78 (s, br, ═NH), 7.7–6.9 (m, Ar-H), 3.29 (s, N–CH$_3$), 3.24 (s, N–CH$_3$), 2.88 (s, O–H). ^{13}C NMR (DMSO, 100 MHz, δ ppm): 158 (C═O), 151(C═O), 149 (C), 148 (C), 136 (C), 27 (N–CH$_3$), 29 (N–CH$_3$), 107 (CH), 117 (CH), 119 (CH), 126 (CH), 128 (C). Anal. calcd for $C_{24}H_{26}N_{10}O_6$: C, 52.36; H, 4.76; N, 25.44, found. C, 51.97; H, 5.16; N, 25.09.

2.3. Synthesis of tetrameric copper(II) complex of H_2L: $[Cu^{II}L]_4{\cdot}2H_2O$ (2.2H_2O)

The ligand 1,3-dimethyl-5-(*o*-phenolate-azo)-6-aminouracil (0.027 g, 0.2 mmol) in DMF (10 mL) was refluxed with stirring at 170 °C for 30 min. Under such conditions, copper(II) chloride dehydrate ($CuCl_2{\cdot}2H_2O$) (0.01 g, 0.1 mmol,) was added. The mixture was further refluxed at the same temperature for an additional 2 h. After cooling to room temperature, the reaction mixture was kept undisturbed for few days for crystallization. The reddish-brown coloured crystals were deposited at the bottom of the beaker and collected by filtration.

Reddish-brown crystal, yield: 60%, m.p. > 300 °C, FT-IR (ν cm^{-1}): 3470 (O–H str), 3321 (N–H), 2928 (Ar–H sym. str.), 1690 & 1638 (C═0), 1540 (C═C), 1466 (N═N), 1264 (C–N), 1062 (C–O str.). Anal. calcd for $C_{48}H_{48}Cu_4N_{20}O_{14}$: C, 41.64; H, 3.49; N, 20.25, found. C, 41.16; H, 3.76; N, 20.11.

2.4. Determination of pK_a of 1

To determine acid dissociation constant (pK_a) values of the ligand, 1,3-dimethyl-5-(*o*-phenolate-azo)-6-aminouracil (H_2L) the simple spectrophotometric half-height method[19] was employed. A series of aqueous buffer/DMSO (20 : 1 v/v) solution mixtures of the ligand at a particular concentration (0.1 μM) was prepared at varying pH 1–12. UV-vis absorptions of the ligand at wavelengths 403, 431 and 447 nm of all the solutions were noted from their respective spectrum. The plot of absorbance *vs.* pH for a particular wavelength determines the pK_a values of the ligand.

2.5. Determination of single crystal X-ray crystallographic structure

While single crystals for the ligand **1** were grown from a methanol solution in red-block shape (0.072 mm × 0.181 mm × 0.197 mm), the same for the tetrameric Cu(II) complex **2.2H_2O** were obtained from *in situ* in red-plate shape (0.010 mm × 0.040 mm × 0.220 mm). The X-ray intensity data were measured using a Bruker D8 Quest with Photon II CPAD detector CCD diffractometer with an Incoatec Microfocus Source Mo Kα radiation (λ = 0.71073 Å) at 100(2) K for **1** and Bruker Kappa Duo APEX2 CCD diffractometer with an Incoatec Microfocus SourceCu Kα radiation (1.54178 Å) at 143(2) K for **2.2H_2O**. Cell refinement and data reduction were performed using the integrated Bruker SAINT software package with a narrow-frame algorithm.[26] Data were corrected for absorption effects by the Multi-Scan method (SADABS).[27] The structures were solved and refined using the Bruker SHELXTL software package,[28] with the space group $P121/c1$, with Z = 4 for **1** and the space group $I41/a$, with Z = 4 for **2.2H_2O**. In order to determine the structures, direct methods

Table 1 Crystallographic data and structure refinement for compounds **H_2L** and **$[Cu^{II}L]_4{\cdot}2H_2O$**

Empirical formula	$C_{24}H_{26}N_{10}O_6$ [**H_2L**]	$C_{48}H_{48}Cu_4N_{20}O_{14}$ [**$Cu_4L_4{\cdot}2H_2O$**]
Colour and shape	Red block	Red plate
Formula weight	550.50	1383.22 g mol^{-1}
Temperature/K	100(2)	143(2)
Crystal system	Monoclinic	Tetragonal
Space group	$P12_1/c1$	$I4_1/a$
a/Å	5.8247(2)	13.2660(4)
b/Å	27.5057(8)	13.2660(4)
c/Å	14.9858(5)	28.9624(12)
α/°	90	90
β/°	90.1504(12)	90
γ/°	90	90
Volume Å^{-3}	2400.90(13)	5097.0(4)
Z	4	4
ρ_{cal}g cm^{-3}	1.523	1.803
μ/mm^{-1}	0.114	2.664
F(000)	1152	2816
Crystal/size/mm^3	0.072 × 0.181 × 0.197	0.010 × 0.040 × 0.220
Radiation	Mo Kα (λ = 0.71073)	Cu Kα (λ = 1.54178)
2θ range for data collection/°	2.60–27.93	3.67–66.63°
Index ranges	$-7 \le h \le 7$, $-36 \le k \le 36$, $-19 \le l \le 19$	$-15 \le h \le 15$, $-15 \le k \le 15$, $-34 \le l \le 34$
Reflections collected	27 162	20 922
Independent reflections	5730 [$R_{(int)}$ = 0.0460]	2262 [$R_{(int)}$ = 0.1424]
Data/restraints/parameters	5730/0/379	2262/3/208
Goodness-of-fit on F^2	1.038	1.065
Final R indexes [$I \ge 2\sigma(I)$]	R_1 = 0.0477, wR_2 = 0.1086	R_1 = 0.0544, wR_2 = 0.1360
Final R indexes [all data]	R_1 = 0.0638, wR_2 = 0.1186	R_1 = 0.0776, wR_2 = 0.1526
Largest diff. peak/hole/e Å^{-3}	0.591/−0.243	0.532/−0.724

or Patterson maps to locate the heavy atoms, followed by difference maps for the light, non-hydrogen atoms were employed. All non-hydrogen atoms were refined with anisotropic thermal parameters. The structures were built using the OLEX2[29] software package. Crystallographic data, refinement and collection parameters for both the structures are listed in Table 1.

2.6. Computational methods

DFT calculations were carried out using the geometries in the crystal structure with the B3LYP functional[30] and the empirical dispersion D3 with Becke–Johnson damping (GD3BJ)[31] and the aug-cc-pVDZ basis set.[32] These calculations have been carried out using the Gaussian-16 program.[33] The electron density of the systems has been analyzed within the quantum theory of atoms in molecules (QTAIM)[34] with the AIMAll[35] program. The topological analysis of the electron density provide the bond, ring and cage critical points. Starting from the bond critical points (BCP) and following a gradient line that finish in a nuclei, the bond path can be defined. The representation of all these properties provides the molecular graphs. In addition, the non-covalent index (NCI) methodology,[36] based on the reduced gradient density (s), was used to characterize those regions of attractive or repulsive interaction. The mutiwfn[37] program was used to calculate the NCI parameters and represented using the Jmol program.[38]

2.7. Magnetic and EPR study

The magnetization of powdered sample **2.2H$_2$O** was measured over the temperature range 1.8–300 K using a Quantum Design SQUID-based MPMSXL-5-type magnetometer. The superconducting magnet was generally operated at a field strength ranging from 0 to 5 T. Measurement sample of compounds were made at a magnetic field of 0.5 T. The SQUID magnetometer was calibrated with the palladium rod sample. Corrections are based on subtracting the sample-holder signal and contribution χ_D estimated from Pascal's constants.[39] The EPR spectra of powdered sample **2.2H$_2$O** were recorded at room temperature and 77 K using a Bruker ELEXSYS E 500 CW-EPR spectrometer operating at the X-band frequency and equipped with an ER 036TM NMR Teslameter and E41 FC frequency counter.

3. Results and discussion

3.1. Synthesis and spectral characterization

The conventional diazotization followed by coupling methods was executed in order to synthesize a new potential ligand, 1,3-dimethyl-5-(*o*-phenolate-azo)-6-aminouracil (H_2L, **1**). The ligand was subjected to synthesize the tetrameric copper(II) complex $[Cu^{II}L]_4{\cdot}2H_2O$ (**2.2H$_2$O**) from the DMF reaction mixture (1 : 1 mole ratio of ligand/Cu^{2+}) under warmed conditions. Suitable crystals for analysis of structures of the ligand and its Cu(II) complex were generated from MeOH and DMF solutions, respectively. The complex possesses Cu_4O_4 cubane-like framework, as shown in Scheme 2.

IR spectra and frequency values of different functionalities of **1** and **2.2H$_2$O** were recorded (see Fig. S1 and S2, ESI;† data in experimental section). The overlapping stretching frequencies of –OH, –NH and Ar–H groups are found in the region 3510–2956 cm^{-1}. The two intense peaks for ν(C═O) stretching vibrations appeared at 1707 cm^{-1} and 1619 cm^{-1} for the ligand and at 1690 cm^{-1} and 1638 cm^{-1} for the complex. Both the peaks are assigned to be the uracil–CO, where former peak is for ^{2}C═O and later is for ^{4}C═O (for numbering, see Scheme 1). The involvement of ^{4}C═O in conjugation with either –N═N– or –C═C– (uracil) makes such discrimination among the uracil–C = O groups. Another two functional groups, –C═C– and –N═N–, which are sensitive to metal coordination, appear at 1531 cm^{-1} and 1476 cm^{-1} for the ligand and at 1540 cm^{-1} and 1466 cm^{-1} for the complex. In addition, two pairs of peaks at 1365 and 1256 cm^{-1} for the ligand and 1376 and 1264 cm^{-1} for the complex can be attributed to the C–N and C–O stretching frequencies.

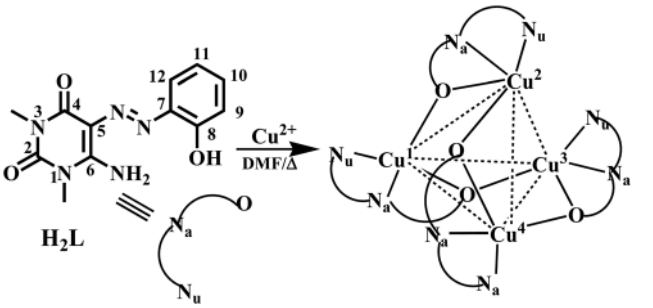

Scheme 2 Formation reaction of $[Cu^{II}L]_4{\cdot}2H_2O$ (**2.2H$_2$O**) (for clarity, water molecules excluded and only $\widehat{ON}_a\widehat{N}_u$ symbol used for the ligand).

The ^{1}H and ^{13}C NMR spectra of the ligand **1** were recorded in the DMSO-d_6 solvent and peaks of different protons and carbons are assigned, as given in the experimental section. The ^{1}H NMR spectrum (Fig. S3, ESI†) reveal that the ligand in DMSO exists in its hydrazone form (Scheme S1: B, ESI†). The hydrazone (═N–NH), phenolic (–OH), and imine (═NH) protons appear as singlet at 12.4 ppm, 11.039 ppm and 8.78 ppm, respectively. The absence of –NH_2 proton and the presence of hydrazone (═N–NH) proton signals in the spectrum rule out the existence of other tautomeric forms (Scheme S1: A, C and D, ESI†). The other protons are in the usual position and in agreement with the literature values.[19] As can be seen in the ^{13}C NMR spectrum (Fig. S4, ESI†) the uracil >C═O carbons signals appear at 159 and 151 ppm and N–CH_3 carbons at 27 and 29 ppm. The other uracil and phenyl carbon signals are in usual positions.[19]

The intense UV-vis band of **1** at 406 nm (ε, 34 000 M^{-1} cm^{-1}) (Fig. 1(a)) in DMF may be originated due to the overlapping of $n \rightarrow \pi^*$ and $\pi \rightarrow \pi^*$ transitions about the ligand moiety. This band shifts to 290 nm (ε, 10 600 M^{-1} cm^{-1}) (Fig. 1(c)) in the complex. In addition, the complex exhibits another three bands (Fig. 1(b) and inset) at 468 nm (ε, 5864 M^{-1} cm^{-1}), 755 nm (ε, 308 M^{-1} cm^{-1}) and 931 nm (ε, 260 M^{-1} cm^{-1}). The band at 468 nm could be assigned to phenolate-to-copper(II) LMCT transitions. The two very low extinction coefficient bands at 755 nm and 931 nm may correspond to d–d transitions associated with distorted square-planar geometry. The results are concomitant with the reported square planar complexes.[40]

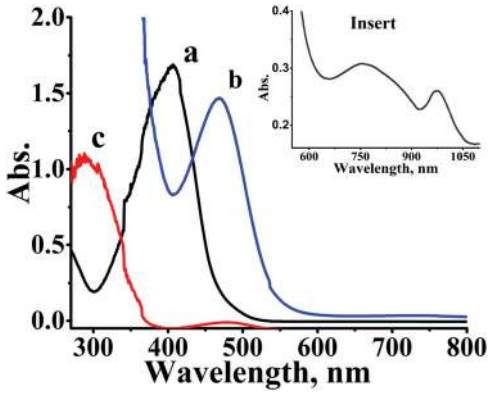

Fig. 1 UV spectra of H_2L **1** (a) and the complex, $[Cu^{II}L]_4{\cdot}2H_2O$, **2.2H$_2$O** (b, c and inset) in DMF.

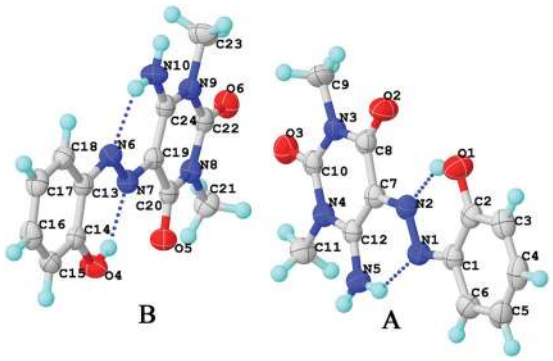

Fig. 2 ORTEP view of H_2L (**1**) (two molecular units: A and B) (50% probability ellipsoids).

In order to get further evidence for which tautomeric forms exclusively present in solution and for their existence in any equilibrium, the pK_a values of the ligand were evaluated. UV-vis spectra of **1** recorded in different buffer solutions of pH 1–12 are appended in Fig. S5 (ESI†). The absorbance λ_{max} at 431 nm at pH 1 corresponding to its hydrazone form (Scheme S1B, ESI†) decreases with the increase in pH to 3.48; it then starts blue-shifting to 403 nm as pH increased to 5.13. Further increasing pH to 12 the features of the spectra become broaden and finally red-shifts to 447 nm. In respect of hydrazone (H_2L) band at 431 nm, the blue-shifted band may be due to the formation of anionic form of hydrazone (HL^-) and the red-shifted band for the formation of hydrazone-phenolic dianion (L^{2-}). To evaluate the pK_a values (pK_1 and pK_2), the absorbance values at 431, 403, and 447 nm were plotted against pH values. The obtained graphs, as shown in Fig. S5B (ESI†), reveal that the absorbance show doubly sigmoid dependence on pH.[41] The half-height method for graphs were followed to calculate the values of pK_1 and pK_2. The mean value of pK_1 was found to be 4.91 and of pK_2 is 9.68 (see Table S1, ESI†), corresponding to the dissociation of the hydrazone and phenolic protons, respectively. The study reveals that the ligand has two dissociable protons and in the course of complexation it coordinates through phenolate–O and deprotonated amino group (–NH$^-$) at the 6-aminouracil group. It is evident that the anionic-hydrazone form switches to the azo-form upon coordination.[19–23]

3.2. Crystal structures

Crystal structure of the ligand (H_2L, **1**) has two molecular units (A & B) in the asymmetric unit of the cell, as can be seen in Fig. 2. Both the units are almost perpendicular in projection. The closest distance between the two molecular units is 2.7683(15) Å, which is measured from O3 atom of the unit A to the plane C20 N8 C22 N9 C24 C19 of unit B. Their bond lengths and bond angles (Table 2 and Tables S2 and S3, ESI†) are bit differed, *e.g.* N1–N2, 1.2920(19) Å in the molecular unit A and 1.2852(19) Å in the molecular unit B. The C–O (C2–O1, 1.349(2) Å) of the phenolic group being single bond in nature is longer than that of the double bonded uracil C–O (C8–O2, 1.228(2) Å; C10–O3, 1.212(2) Å) groups. The uracil C–O (C10–O3) bond which is in conjugation with the uracil C–C (C7–C12) double band is longer than the non-conjugated one. The bond length of C–C (C7–C12, 1.401(2) Å) double bond is comparable with the C–C bonds of the phenyl group (Tables S2 and S3, ESI†). H-atoms of phenolic–OH and uracil–NH_2 groups of the molecular units A and B play pivotal role in forming intra- and inter-molecular H-bonds (Fig. S6, ESI†). For a particular unit they associate in intra-molecular H-bonding with the azo-N atoms forming 6-membered closed rings. Outward uracil–NH establishes a link with the phenolic–OH of a unit, whereas uracil–O with outward uracil–NH of other unit makes the network looking as if molecular paddle-wheeled. The H-bonding data are listed in Table S4 (ESI†). The shortest H-bond is found in the molecular unit A among phenolic-H atom and azo-atom (O1H–N2, 1.763 Å). The most characteristic feature of the structure is the pi–pi stacking of these molecular units with each molecule to form a separate stuck, which forms layers parallel to the (010) plane (Fig. S7, ESI†). The arrangement of stacks within each layer is of tweed type in nature.

With the ligand, Cu(II) forms a complex that has tetranuclear doubly opened 4+2 cubane-like structure,[12] $[Cu^{II}L]_4{\cdot}2H_2O$, (**2.2H$_2$O**). The molecular view of the **2.2H$_2$O** is shown in Fig. 3 and its bond lengths and bond angles are tabulated in Table 2 and Tables S5 and S6 (ESI†). The molar ratio of ligand to Cu(II) is 1 : 1, where ligand acts as a dianionic tridentate ligand. In the ligand frame the –OH and –NH_2 groups are in opposite sides of the azo-functionality (*E*-configuration) but in the complex they become *cis*-oriented for coordinating Cu(II). The azo –N=N– bond length (1.282(5) Å) of the ligand in the complex is bit less in comparison with the free ligand units (Fig. 1). The uracil –NH group is shortened by 0.019 Å and the double bond C7–C12 is increased by 0.034 Å, which are in conjugation with the –N=N– group, indicating the existence of chelate ring current on the chelate frame, –NH–C–C–N=N–upon coordination to Cu(II). The ligand forms six- and five-membered chelate rings around Cu(II) with a common azo-coordination link. Both the rings constitute a plane, C1O1Cu1N5C12C7N2N1C6, which is normal to the plane normal (90.223(7)). The ligand frames at the Cu(II) centers are almost perpendicular to each other. The four Cu(II) ions in the complex entity are bridged through phenolate–O (μ_2-O) of the ligand moiety with a Cu–O–Cu bridging angle of

Table 2 Selective important bond lengths (Å) and bond angles (°) of H_2L and $[Cu_4L_4]\cdot 2H_2O$

H_2L					
Molecule A		Molecule B		$[Cu_4L_4]\cdot 2H_2O$	
Bonds	Lengths (Å)	Bonds	Lengths (Å)	Bonds	Length (Å)
N1–N2	1.2920(2)	N6–N7	1.2852(2)	N1–N2	1.282(5)
C2–O1	1.349(2)	C14–O4	1.356(2)	Cu1–N5	1.900(4)
C8–O2	1.228(2)	C20–O5	1.234(2)	Cu1–N1	1.920(4)
C10–O3	1.212(2)	C22–O6	1.212(2)	Cu1–O1	1.940(3)
C7–C12	1.401(2)	C19–C24	1.410(2)	Cu1–O1^{i}	1.969(3)
C1–N1	1.410(2)	C13–N6	1.412(2)	C1–O1	1.347(6)
C7–N2	1.365(2)	C19–N7	1.366(2)	C7–C12	1.435(6)
				C7–N2	1.337(6)
				C12–N5	1.306(6)
Bonds	Angles (°)	Bonds	Angles (°)	Bonds	Angles (°)
N2–N1–C1	113.27(14)	N7–N6–C13	113.36(13)	N5–Cu1–N1	91.39(16)
N1–N2–C7	121.14(14)	N6–N7–C19	120.53(14)	N1–Cu1–O1	84.39(15)
				N1–Cu1–O1^{i}	167.05(15)
				N5–Cu1–O1	173.15(15)
				N5–Cu1–O1^{i}	95.74(15)
				O1–Cu1–O1^{i}	117.6(4)
				Cu1–O1–Cu1^{i}	122.14(16)

$^{i}\frac{1}{4} + y, \frac{1}{4} - x, 9/4 - z$.

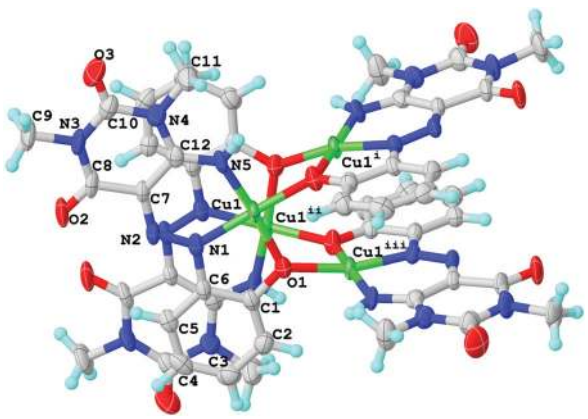

Fig. 3 ORTEP view of the tetrameric form of copper(II) complexes of H_2L, $[Cu^{II}L]_4$ (50% probability ellipsoids; symmetry codes, (i) $\frac{1}{4} + y, \frac{1}{4} - x, 9/4 - z$; (ii) $-x, \frac{1}{2} - y, +z$; (iii) $\frac{1}{4} - y, \frac{1}{4} + x, 9/4 - z$). Crystal H_2O molecule not included for clarity.

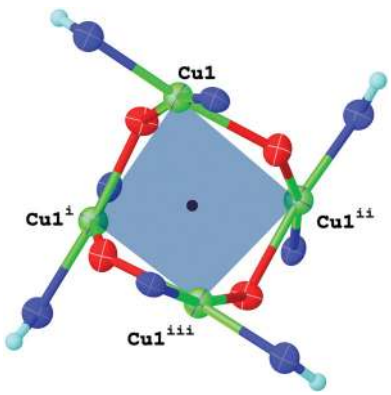

Fig. 4 Tetrahedral arrangement of the Cu_4 cluster.

122.13(15)°. The coordination environment about Cu(II) is distorted square planar, $\tau_4 = 0.135$ and $\tau_4' = 0.1214$ (α = N1–Cu1–O1 = 167.05(15) and β = N5–Cu1–O1 = 173.15(15)).[42] The *cis*-angles are nearly right angles varied from 84.39(15)° (N1–Cu1–O1) to 95.74(15)° (N5–Cu1–O1^{i}) and the two nearly linear *trans*-angles are 173.15(15)° for N5–Cu1–O1 and 167.05(15)° for N1–Cu1–O1^{i} (Table 2). The four equivalent Cu(II) ions are on the vertices of a nearly perfect tetrahedron, which is understood from the Cu1-plane centroid-Cu1 angle of 108.258(16)° (see Fig. 4). The center of the tetrahedron is at Wyckoff position 4a with S_4 symmetry. The four Cu···Cu (3.426(11) Å) and two Cu···Cu (3.498(13) Å) distances are alike within the Cu_4 tetrahedron, forming a Cu_4O_4 cubane-like framework. According to Tercero *et al.*[12a] classification of Cu_4 cubane-like structures, the present structure has four short and two long Cu···Cu distances with an S_4 symmetry, making the cluster in the family of 4+2-type cubane structures. In comparison to Cu···Cu distances of 4+2 cubane systems,[12d] the present structure has the longest Cu···Cu distances, but the difference between short and long bonds is minimal (0.072 Å) except the complex reported by Liu *et al.*[12c] Moreover, the distances are quite short while comparing with the reported cluster (Cu–Cu, 4.15- 4.80 Å) containing similar ligand frames (a comparative study given in Table S7, ESI†).[24a] They differ in magnetic behaviors as well, which is elaborately discussed in the following section.

3.3. Non-covalent interactions

The X-ray structure of molecule **1** shows two intramolecular bonds connecting the two nitrogen atoms of the azo group with the hydroxyl and amino groups (Fig. 2). The AIM analysis shows the corresponding BCPs connecting the interacting groups and the NCI plot isosurfaces confirm the existence of intramolecular BCPs (Fig. S8, ESI†). The crystal packing of **1** is composed of two

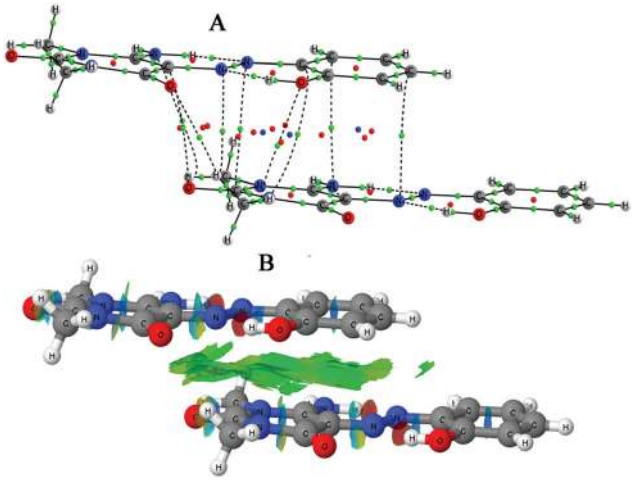

Fig. 5 (A) Molecular graph and (B) NCI plot of the stacked dimer of the independent molecule B.

types of interactions. On the one hand, the molecules are located forming a displaced stacking (Fig. 5). The molecular graph of this dimer shows the presence of a number of critical points connecting the two molecules (Fig. 5A) and a NCI plot isosurface with color green (Fig. 5B) as indication of moderate stabilization in the interaction. The calculated interaction energies are −69.5 and −77.3 kJ mol^{-1} for the molecules A and B (Fig. 1), respectively. On the other hand, the molecules are also in an angular disposition (Fig. 6) with the oxygen atom of the carbonyl group of one molecule A pointing towards the carbon atom of the same group in another molecule B, similar to the one described in the Bürgi-Dunning trajectory,[43] which corresponds to a tetrel bonding interaction.[44] The molecular graph of this dimer shows some additional bond critical points between the methyl groups of one of the molecules and the carbonyl groups of the other. In the NCI plot, the isosurfaces present green color as confirmation of the moderate interaction between the two molecules. The stabilization of this interaction is −43.8 kJ mol^{-1}.

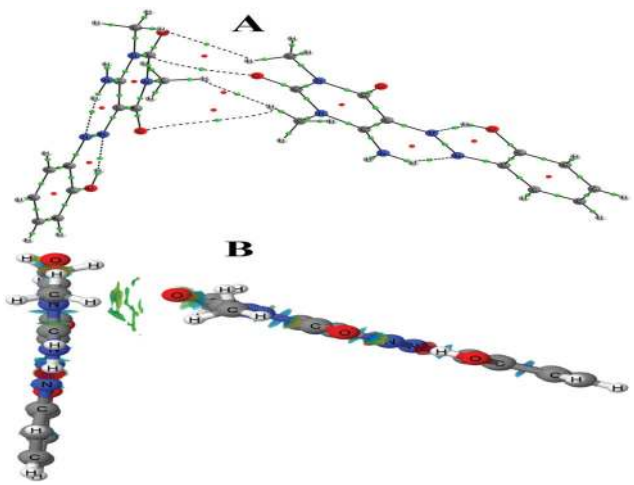

Fig. 6 (A) Molecular graph and (B) NCI plot of the angular dimer by molecules A and B.

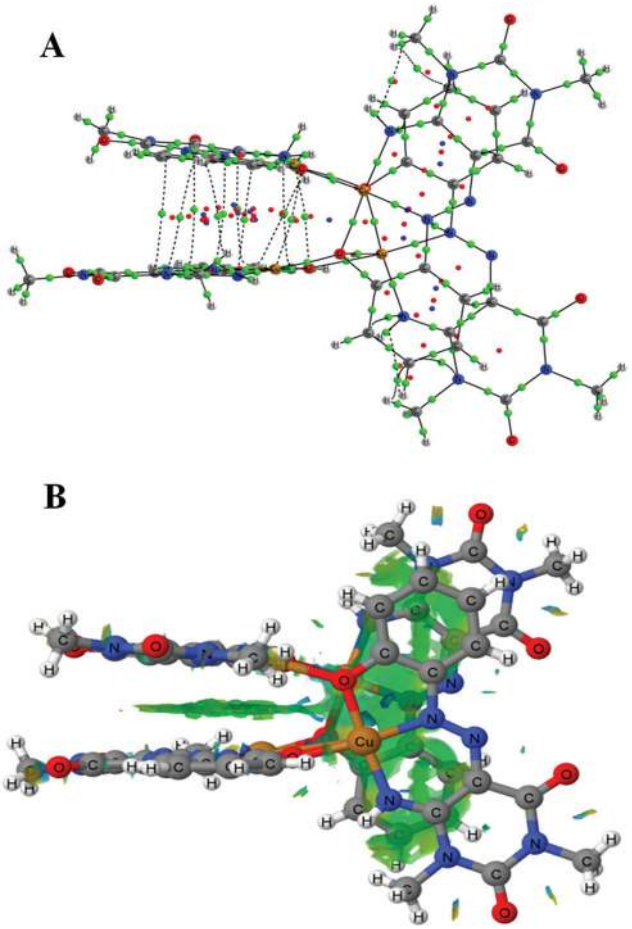

Fig. 7 (A) Molecular graph and (B) NCI plot of complex **2.2H$_2$O**. The location of the bond, ring and cage critical points is indicated with green, red and blue dots in the molecular graph.

The AIM analysis (Fig. 7A) of the complex **2.2H$_2$O** shows a number of bond paths connecting the two stacked subunits. The electron density values of the BCPs connecting the two subunits have the typical signature of weak non-covalent interactions: values of ρ smaller than 0.01 au and positive values of the $\nabla^2\rho$ and H. The NCI plot isosurfaces between the two stacked subunits are typical of stacked system with small values of the curvature, λ^2, as indicated by the green color in Fig. 7B. The copper atoms are involved in five interactions each: two strong Cu–N ($\rho_{BCP} \sim 0.11$ au) and three Cu–O bonds (two strong, $\rho_{BCP} \sim 0.08$–0.09 au and one weak, $\rho_{BCP} = 0.011$ au).

3.5. Magnetism and EPR study

On the basis of structural data, from the viewpoint of magnetochemistry, compound **2.2H$_2$O** can be defined as a tetranuclear Cu(II) unit linked through phenolate bridges. The magnetic properties of **2.2H$_2$O** were then investigated over the temperature range of 1.8–300 K. Plots of magnetic susceptibility χ_m and $\chi_m T$ product *vs.* T (χ_m is the molar magnetic susceptibility for four Cu^{II} ions) are given in Fig. 8. For **2.2H$_2$O**, the $\chi_m T$ value at room temperature is much below this expected for four magnetically isolated copper(II) ions [$\chi_m T = 4(N\beta^2 g^2/3k)S(S+1) = 1.5$ cm^3 K mol^{-1},

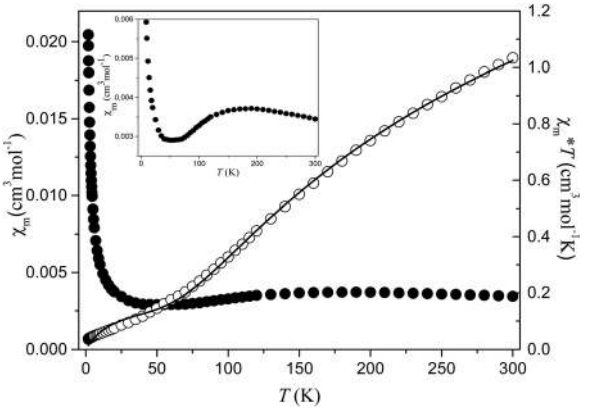

Fig. 8 Temperature dependence of experimental χ_m (●) and χ_mT (○) (χ_m per 4Cu^{II} atoms) for **2.2H$_2$O**. The solid line is the calculated curve derived from eqn (1)–(4). The inset shows a closer view of χ_m *vs.* T plot for **2.2H$_2$O**.

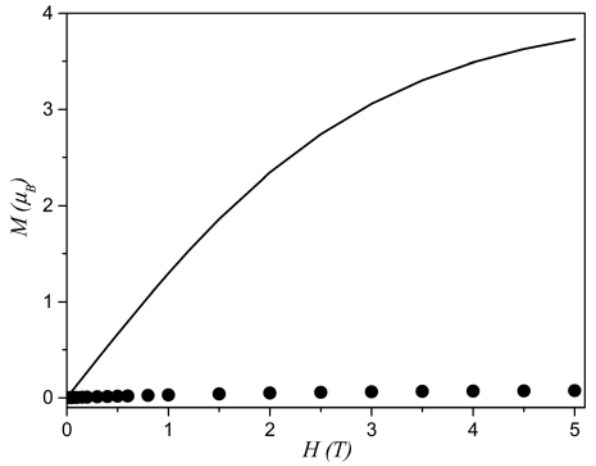

Fig. 9 Field dependence of the magnetization (M per Cu_4 entities) for **2.2H$_2$O**. The solid line is the Brillouin function curve for the system of four uncoupled spins with $S = {}^1/_2$ and g = 2.0.

assuming g = 2.1 and $S = \frac{1}{2}$, where N, β, g, k, S and T have their usual meanings,[1a] being equal to 1.10 cm^3 K mol^{-1}]. Upon cooling, the χ_mT continuously decreases reaching almost zero at 1.8 K. These features are indicative of a strong antiferromagnetic coupling between the copper(II) ions in **2.2H$_2$O** that leads to a low-lying spin state (S = 0). Additionally, the susceptibility curve for **2.2H$_2$O** exhibits the maximum that confirms the presence of a strong antiferromagnetic ordering with a Néel temperature (T_N) about 200 K (Fig. 8). The rapid increase of χ_m at the low temperatures is due to the presence of a small amount of paramagnetic impurities ($S = \frac{1}{2}$).

The variation of the magnetization (M) with respect to the field (H), at 2 K, also confirms the nature of the ground state in **2.2H$_2$O**. The results are shown in Fig. 9, where the molar magnetization M (per Cu_4 entities) is expressed in μ_B units. The complex does not reach the saturation in the applied field range and the magnetization value in 5 T is much below 1μ_B. The magnetization curve for **2.2H$_2$O** was reproduced by the equation $M = g\beta SNB_s(x)$ ($S = 4S_{Cu}$), where $B_s(x)$ is the Brillouin function and $x = g\beta H/kT$.[1a] The experimental values are very inferior compared to those calculated using the Brillouin function for four non-interacting copper(II) ions. This further indicates that **2.2H$_2$O** behaves as antiferromagnet.

$$H = -2J_1(\hat{S}_{Cu1}\hat{S}_{Cu1^i} + \hat{S}_{Cu1^i}\hat{S}_{Cu1^{iii}} + \hat{S}_{Cu1^{iii}}\hat{S}_{Cu1^{ii}} + \hat{S}_{Cu1^{ii}}\hat{S}_{Cu1}) - 2J_2(\hat{S}_{Cu1}\hat{S}_{Cu1^{iii}} + \hat{S}_{Cu1^i}\hat{S}_{Cu1^{ii}}) \quad (1)$$

To avoid overparametrization, we assumed that the exchange coupling constants within the cubane [Cu_4O_4] core that involved short Cu···Cu distances are equivalent and described by J_1, whereas those that involved long Cu···Cu distances are described by J_2 (Fig. 4).

The magnetic susceptibility of **2.2H$_2$O** was therefore fitted according to the following equation (eqn (2)), as the sum of two independent contributions, namely, one due to the tetracopper(II) blocks with the $S = \frac{1}{2}$ spins ($\chi_{m(cubane)}$), and the other one due to eventually paramagnetic monomeric impurities ($\chi_{m(para)}$), in addition to a possible temperature independent term ($\chi_{(N\alpha)}$), with a typical value for copper(II) ions of 60 × 10^{-6} cm^3 mol^{-1}.

$$\chi_m = (1 - \rho)\chi_{m(cubane)} + \rho\chi_{m(para)} + \chi_{N\alpha} \quad (2)$$

The magnetic susceptibility per cubane [Cu_4O_4] core, $\chi_{m(cubane)}$, derived from the van Vleck formula assuming an equal g value for the four copper(II) ions, is given by eqn (3):

$$a\chi_{m(cubane)} = \frac{2N\beta^2g^2}{kT}\frac{\exp[(2J_2 - J_1)/kT] + 2\exp(J_2/kT) + 5\exp[(J_1 - 2J_2)/kT]}{1 + \exp[(2J_2 - 2J_1)/kT] + 3\exp[(2J_2 - J_1)/kT] + 5\exp[(J_1 - 2J_2)/kT + 6\exp(J_2/kT)]} \quad (3)$$

Magnetostructural correlations for different families of polynuclear complexes containing a Cu_4O_4 core are known. These complexes are classified according to their numbers of short and long Cu···Cu distances as 2+4, 4+2 or 6+0. In the crystal structure of compound **2.2H$_2$O**, four copper(II) ions (Cu_1, Cu_1^i, Cu_1^{ii}, and Cu_1^{iii}) occupy alternate cubane vertices and there are six exchange interactions between the four copper(II) centers. Considering the presence of four short (3.426 Å) and two rather long (3.498 Å) Cu···Cu separations in **2.2H$_2$O**, the cubane [Cu_4O_4] core can be classified within the 4+2 category and analyzed using the spin Hamiltonian given in eqn (1):[12,45]

where all parameters have their usual meaning. The contribution $\chi_{m(para)}$ is expected to follow a Curie–Weiss model for the $S = \frac{1}{2}$ spins (eqn (4)):

$$\chi_{m(para)} = \frac{Ng^2\beta^2}{4kT} \quad (4)$$

The intermolecular interactions between copper(II) ions in neighboring molecules are omitted because of the rather long Cu···Cu distances and overparametrization. The paramagnetic monomeric impurity ρ was introduced to obtain satisfactory results.[1a] A least-squares fitting of the experimental data leads to the following values: J_1 = −110.1(1) cm^{-1}, J_2 = −27.1(2) cm^{-1},

$g = 2.09(1)$ and $\rho = 8.1\%$ ($R = 6.63 \times 10^{-4}$). The criterion applied to determine the best fit was based on the minimization of the sum of squares of the deviation, $R = \Sigma(\chi_{exp}T - \chi_{calc}T)^2/\Sigma(\chi_{exp}T)^2$. The calculated curve (solid lines in Fig. 8) matches very well the experimental magnetic data in the whole temperature range. The obtained values of J_1 and J_2 indicate an antiferromagnetic coupling between the copper(II) ions transmitted through μ-phenolate linkers within the tetracopper(II) cluster in **2.2H$_2$O**.

Previous studies of hydroxo-, alkoxo- and phenoxo-bridged copper(II) compounds[45–47] indicate that the nature and the strength of the overall coupling in such systems can be influenced by the Cu···Cu distances and Cu–O–Cu angles. Generally, the longer the Cu···Cu distance, the weaker the exchange interaction. When the Cu–O–Cu angle is $<97.5^\circ$, ferromagnetic interactions can be expected, whereas in the case of this angle being more than 97.5° the interaction *via* the Cu–O–Cu pathway is mostly antiferromagnetic, with an increasing magnitude as the angle increases.[12,25,46–48] Although the Cu–O–Cu angles and Cu···Cu distances are the most crucial geometrical parameters, the coupling constants can also be modulated by the other structural features. The values of J_1 and J_2 obtained for **2.2H$_2$O** are larger than several earlier reported values for this parameters in alkoxo- and phenoxo bridged 4+2 Cu_4O_4 cubanes.[12,45] This fact is certainly associated with the relatively large values of the Cu–O–Cu angles (122.13°) and rather long copper···copper separations (3.426 and 3.498 Å) observed in **2.2H$_2$O** to be compared with those of the literature.[12,25,45] However, the calculated J_2 parameter for **2.2H$_2$O** has a negative value in contrast to weakly ferromagnetic interactions generally found in the literature. It was proposed that these interactions are practically independent of the geometrical parameters.[12a] In general, the magnetic behavior of **2.2H$_2$O** is in agreement with the majority of alkoxo- and phenoxo-bridged tetranuclear copper(II) compounds. With slight differences in structural features of **2.2H$_2$O**, such different coordination geometries of copper atoms and double-open 4+2 cubane-like structures may also cause some distinction in the magnetic properties in order to relate complexes involving the [Cu_4O_4] core. Moreover, a compound obtained on the basis of the azo-derivative of 6-aminouracil is already known in the literature. This compound forms a quasi-tetrahedral Cu_4 cluster linked through carboxylate bridges.[24a] Despite some structural similarities, both compounds also show some differences in the structure that make them differ in their magnetic behavior. For **2.2H$_2$O**, the calculated J parameters has negative values in contrast to ferromagnetic interactions found in the literature.[24a] The magnitude and the sign of a magnetic exchange interaction depends on the overlap of the magnetic orbitals centered on adjacent copper(II) ions.[46a,b,47] The mechanism of antiferromagnetic coupling between the Cu···Cu centers in **2.2H$_2$O** is a result of the interaction of the $d_{x^2-y^2}$ orbitals positioned in the square base *via* the phenolate oxygen atoms. The weaker overlap of magnetic orbitals of the metals in the earlier reported cluster arise from a trigonal character of copper(II) environment and the electron delocalization on the d_{z^2} magnetic orbitals. This causes a reduction of the antiferromagnetic contribution, which leads ultimately to an overall ferromagnetic behavior. For a *syn-anti* conformation of the (Cu–O–C–O–Cu) bridges,[24a] the orbitals are unfavorably oriented to give a strong overlap. Additionally, the angles between *syn* Cu–O bonds and *anti* Cu–O bonds show, in the quasi-tetrahedral Cu_4 cluster, an average value of 97.8°, which is significantly low and is probably the main reason for the overall ferromagnetic interaction in this case.

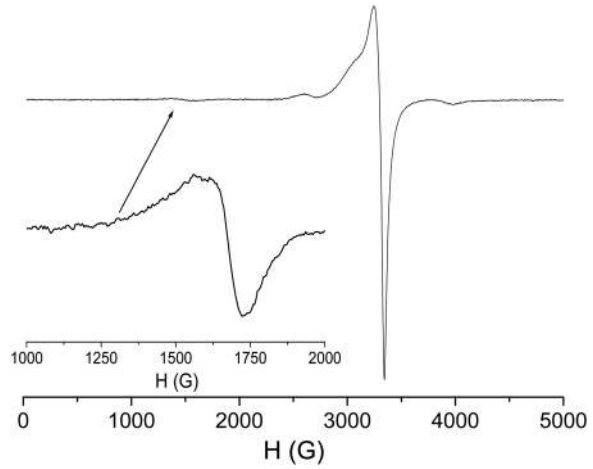

Fig. 10 EPR (X-band) spectrum of powdered sample **2.2H$_2$O** at 77 K. The insets show forbidden line $\Delta M_S = 2$.

The EPR spectra of **2.2H$_2$O** additionally confirm the properties determined by direct magnetic measurements (Fig. 10). The X-band EPR spectra of powdered sample show no significant difference between room temperature and 77 K. Compound **2.2H$_2$O** is a tetranuclear Cu(II) unit ($S = {}^1/_2$), in which antiferromagnetic interactions lead to a ground state ($S = 0$). The EPR spectra of **2.2H$_2$O** are indicative of $S = \frac{1}{2}$ and half-field transition is also observed. These signals are devoid of any hyperfine structure. The EPR spectrum of **2.2H$_2$O** displays two superimposed bands and one strong absorption at ~3200 G ($g_\parallel = 2.21$ and $g_\perp = 2.10$). The observed trend in EPR parameters $g_\parallel > g_\perp > 2.04$ displays a $d_{x^2-y^2}$ ground state with distorted square planar geometry for copper(II) ions.[49] The g-values are related to exchange-coupling parameter (G) expressed as $G = (g_\parallel - 2.0023)/(g_\perp - 2.0023)$. The value of the exchange intramolecular coupling parameter, G, is equal to 2.13 for **2.2H$_2$O** and is lower than the value of 4.0, showing significant exchange coupling at the polycrystalline state.[25c]

4. Conclusions

The newly designed 6-aminouracil-phenylazo ligand with an *o*-hydroxy group is found in chelate-cum-bridging mode with copper(II). The phenolate-μ_2-O nature in the ligand frame leads to the formation of a discrete tetranuclear copper(II) cluster, where each Cu(II) possesses a distorted square planar geometry involving the $d_{x^2-y^2}$ orbital in the ground state. The cluster has a 4+2 doubly opened Cu_4O_4 cubane-like framework. Interestingly, the four Cu(II) ions occupy the alternate corner of the cubane-forming tetrahedron with an S_4 symmetry. The ligand exhibits strong tetrel bonding interactions among the two molecular units, whereas the complex has weak interactions among the two stacked

subunits. The magnetic studies have disclosed a strong antiferromagnetic interaction within the Cu_4O_4 cluster of **2.2H$_2$O**. The nature and magnitude of the magnetic coupling were discussed on the basis of structural parameters and compared with those of related alkoxo- and phenoxo-bridged 4+2 Cu_4O_4 cubanes. Thus, we present the tetrahedron Cu_4O_4 cluster compound as a noble antiferromagnetic material for prospective applications in materials science.

Authors contributions

NBN: designing problem, synthesis, isolation, crystallization, spectroscopic data collection and characterization; AP: crystallization and spectroscopic data collection; SR: spectroscopic data collection; JK: magnetic data collection and calculation, EPR study and writing; RG: Crystal data collection and structure modification; IA: non-covalent studying and writing; TKM: designing problem, data collection, writing and organizing the manuscript.

Conflicts of interest

There are no conflicts on this research work among the authors to declare.

Acknowledgements

The authors: NBN, AP, SR, and TKM are thankful to the Department of Chemistry, NIT Agartala for availing research facilities. NBN is grateful to NIT Agartala for receiving institutional fellowship from MHRD, Govt. of India. SR is thankful to BRNS, DAE, Govt. of India, sanction no.: 36(4)/14/12/2018-BRNS/36235 for financial support.

References

1 (*a*) O. Kahn, *Molecular Magnetism*, VCH Publications, New York, 1993; (*b*) in *Single-Molecule Magnets and Related Phenomena*, ed. R. Winpenny, Springer, New York, 2006; (*c*) P. Albores and E. Rentschler, *Angew. Chem., Int. Ed.*, 2009, **48**, 9366–9370; (*d*) S. Sasmal, S. Hazra, P. Kundu, S. Majumder, N. Aliaga-Alcalde, E. Ruiz and S. Mohanta, *Inorg. Chem.*, 2010, **49**, 9517–9526; (*e*) H.-L. Sun, Z.-M. Wang and S. Gao, *Chem. – Eur. J.*, 2009, **15**, 1757–1764; (*f*) O. Kahn and T. Mallah, *J. Chem. Soc., Dalton Trans.*, 1989, 1117–1126; (*g*) A. Banerjee, R. Singh, E. Colacio and K. K. Rajak, *Eur. J. Inorg. Chem.*, 2009, 277–284; (*h*) M.-L. Boillot, O. Kahn, C. J. O'Connor, J. Gouteron, S. Jeannin and Y. Jeannin, *J. Chem. Soc., Chem. Commun.*, 1985, 178–180.

2 (*a*) K. Ikeda, S.-I. Ohkoshi and K. Hashimoto, *Chem. Phys. Lett.*, 2001, **349**, 371–375; (*b*) C. Train, T. Nuida, R. Gheorghe, M. Gruselle and S. I. Ohkoshi, *J. Am. Chem. Soc.*, 2009, **131**, 16838–16843.

3 (*a*) B. S. Sran, S. Sharma, F. Pointillart, O. Cador and G. Hundal, *Inorg. Chem.*, 2020, **59**, 9227–9238; (*b*) D. Gatteschi and R. Sessoli, *Angew. Chem., Int. Ed.*, 2003, **42**, 268–297.

4 (*a*) O. Kahn, J. Larionova and J. V. Yakhmi, *Chem. – Eur. J.*, 1999, **5**, 3443–3449; (*b*) G. Férey, *Nat. Mater.*, 2003, **2**, 136–137.

5 G. L. J. A. Rikken and E. Raupach, *Nature*, 1997, **390**, 493–494.

6 (*a*) in *Transition Metals in Supramolecular Chemistry, in Perspectives in Supramolecular Chemistry*, ed. J.-P. Sauvage, vol. 5, Wiley, London, 1999; (*b*) M. J. Zaworotko, *J. Am. Chem. Soc.*, 2010, **132**, 7821–7822; (*c*) J. J. Zhang, L. Wojtas, R. W. Larsen, M. Eddaoudi and M. J. Zaworotko, *J. Am. Chem. Soc.*, 2009, **131**, 17040–17041; (*d*) M. Nayak, A. Jana, M. Fleck, S. Hazra and S. Mohanta, *CrystEngComm*, 2010, **12**, 1416–1421.

7 (*a*) R. H. Holm, P. Kennepohl and E. I. Solomon, *Chem. Rev.*, 1996, **96**, 2239–2314; (*b*) I. A. Koval, P. Gamez, C. Belle, K. Selmeczi and J. Reedijk, *Chem. Soc. Rev.*, 2006, **35**, 814–840.

8 E. M. Johnston, S. Dell'Acqua, S. Ramos, S. R. Pauleta, I. Moura and E. I. Solomon, *J. Am. Chem. Soc.*, 2014, **136**, 614–617.

9 C. Lu, K. Laws, A. Eskandari and K. Suntharalingam, *Dalton Trans.*, 2017, **46**, 12785.

10 (*a*) S. Wang, S. J. Trepanier, J. C. Zheng, Z. Pang and M. J. Wagner, *Inorg. Chem.*, 1992, **31**, 2118; (*b*) G. Zhang, G. Proni, S. Zhao, E. C. Constable, C. E. Housecroft, M. Neuburger and J. A. Zampese, *Dalton Trans.*, 2014, **43**, 12313–12320; (*c*) L. Liu, Y.-F. Peng, X.-X. Lv, K. Li, B.-L. Li and B. Wu, *CrystEngComm*, 2016, **18**, 2490–2499; (*d*) O. V. Nesterova, O. E. Bondarenko, A. J. L. Pombeiro and D. S. Nesterov, *Dalton Trans.*, 2020, **49**, 4710–4724.

11 C. Hou, Y.-L. Bai, X. L. Bao, L. Xu, R.-G. Lin, S. Zhu, J. Fang and J. Xu, *Dalton Trans.*, 2015, **44**, 7770–7773.

12 (*a*) J. Tercero, E. Ruiz, S. Alvarez, A. Rodríguez-Fortea and P. Alemany, *J. Mater. Chem.*, 2006, **16**, 2729–2735; (*b*) P. Seppälä, E. Colacio, A. J. Mota and R. Sillanpää, *Inorg. Chem.*, 2013, **52**, 11096–11109; (*c*) M.-L. Liu, J.-M. Dou, J.-Z. Cui, D.-C. Li and D.-Q. Wang, *J. Mol. Struct.*, 2012, **1011**, 140–144; (*d*) E. Gungor, H. Kara, E. Colacio and A. J. Mota, *Eur. J. Inorg. Chem.*, 2014, 1552–1560; (*e*) E. Gungor and H. Kara, *J. Struct. Chem.*, 2015, **56**, 1646–1652; (*f*) S. S. P. Dias, M. V. Kirillova, V. André, J. Kłak and A. M. Kirillova, *Inorg. Chem.*, 2015, **54**, 2504–5212; (*g*) S. Sagar, S. Sengupta, S. K. Chattopadhyay, A. J. Mota, A. E. Ferao, E. Riviere, W. Lewis and S. Naskar, *Dalton Trans.*, 2017, **46**, 1249–1259.

13 L. Baldrati, O. Gomonay, A. Ross, M. Filianina, R. Lebrun, R. Ramos, C. Leveille, F. Fuhrmann, T. R. Forrest, F. Maccherozzi, S. Valencia, F. Kronast, E. Saitoh, J. Sinova and M. Kläui, *Phys. Rev. Lett.*, 2019, **123**, 177201.

14 A. Jamaledini, M. R. Mohammadizadeh and S. H. Mousavi, *MonatsheftefürChemie - Chem. Mon.*, 2018, **149**, 1421–1428.

15 J. L. Bernier, J. P. Henichart, V. Warin, C. Trentesaux and J. C. Jardillier, *J. Med. Chem.*, 1985, **28**, 497.

16 B. H. Lee, J. H. Shin and M. K. Lim, *Bull. Korean Chem. Soc.*, 1997, **18**, 734.

17 Z. Seferoğlu, *ARKIVOC*, 2009, 42–57.

18 (*a*) J. Sivamani and A. Siva, *Sens. Actuators, B*, 2017, **242**, 423–433; (*b*) A. Purkayastha, D. Debnath, R. Ganguly and T. K. Misra, *J. Chem. Crystallogr.*, 2017, **47**, 101–109.

19 (*a*) D. Debnath, S. Roy, B.-H. Li, C.-H. Lin and T. K. Misra, *Spectrochim. Acta*, 2015, **140A**, 185–197; (*b*) D. Debnath, A. Purkayastha, R. Choudhury and T. K. Misra, *Ind. Chem. Soc.*, 2016, **93**, 989–998; (*c*) D. Debnath, S. Roy, A. Purkayastha, A. Bauzá, R. Choudhury, R. Ganguly, A. Frontera and T. K. Misra, *J. Mol. Struct.*, 2017, **1141**, 225–236.

20 (*a*) D. Debnath, A. Purkayastha, R. Choudhury and T. K. Misra, *J. Chin. Chem. Soc.*, 2016, **63**, 580–589; (*b*) D. Debnath, A. Purkayastha, A. Kirillov, R. Ganguly and T. K. Misra, *J. Mol. Struct.*, 2017, **1150**, 118–126.

21 (*a*) A. Purkayastha, D. Debnath, S. Roy, A. Bauzá, R. Choudhury, A. Frontera and T. K. Misra, *Eur. J. Inorg. Chem.*, 2016, 5585–5593; (*b*) A. Purkayastha, A. Frontera, R. Ganguly and T. K. Misra, *J. Mol. Struct.*, 2018, **1170**, 70–81.

22 A. Purkayastha, D. Debnath, M. Majumder, J. Ortega-Castro, A. M. Kirillov, R. Ganguly, J. Kłak, A. Frontera and T. K. Misra, *Inorg. Chim. Acta*, 2018, **482**, 384–394.

23 A. Purkayastha, S. Dhar, S. P. Mondal, A. Franconetti, A. Frontera, R. Ganguly, A. M. Kirillov and T. K. Misra, *CrystEngComm*, 2020, **22**, 829.

24 (*a*) E. Colacio, J.-P. Costes, R. Kivekãs, J.-P. Laurent and J. Ruiz, *Inorg. Chem.*, 1990, **29**, 4240; (*b*) E. Colacio, J.-P. Costes, R. Kivekãs, J.-P. Laurent, J. Ruiz and M. Sundberg, *Inorg. Chem.*, 1991, **30**, 1475–1479; (*c*) J. M. Moreno, J. Ruiz, J. M. Dominguez-Vera and E. Colacio, *Inorg. Chim. Acta*, 1993, **208**, 111–115; (*d*) J. M. Moreno, J. Ruiz, J. M. Dominguez-Vera, E. Colacio, D. Galisteo and R. Kivekãs, *Polyhedron*, 1994, **21**, 203.

25 (*a*) M. Fondo, A. M. García-Deibe, M. Corbella, E. Ruiz, J. Tercero, J. Sanmartín and M. R. Bermejo, *Inorg. Chem.*, 2005, **44**, 5011–5020; (*b*) J. Chakraborty, S. Thakurta, G. Pilet, D. Luneau and S. Mitra, *Polyhedron*, 2009, **28**, 819–825; (*c*) S. K. Patel, R. N. Patel, Y. Singh, Y. P. Singh, D. Kumhar, R. N. Jadeja, H. Roy, A. K. Patel, N. Patel, N. Patel, A. Banerjee, D. Choquesillo-Lazarte and A. Gutierrez, *Polyhedron*, 2019, **161**, 198–212.

26 SAINT, Data Reduction and Frame Integration Program for the CCD Area-Detector System, Bruker Analytical X-ray Systems, Madison, Wisconsin, USA, 1997–2006.

27 G. M. Sheldrick, *SADABS, Program for Area Detector Adsorption Correction, Institute for Inorganic Chemistry*, University of Göttingen, Göttingen, Germany, 1996.

28 *SHELXTL-2014/6 (Sheldrick, 2014)*, Bruker AXS Inc., Madison, WI, USA, 2014.

29 O. V. Dolomanov, L. J. Bourhis, R. J. Gildea, J. A. K. Howard and H. Puschmann, *OLEX2, J. Appl. Crystallogr.*, 2009, **42**, 339–341.

30 (*a*) A. D. Becke, Density–Functional Thermochemistry. III. The Role of Exact Exchange, *J. Chem. Phys.*, 1993, **98**, 5648–5652; (*b*) C. Lee, W. Yang and R. G. Parr, Development of the Colle-Salvetti Correlation-Energy Formula into a Functional of the Electron Density, *Phys. Rev. B: Condens. Matter Mater. Phys.*, 1988, **37**, 785–789.

31 S. Grimme, S. Ehrlich and L. Goerigk, Effect of the damping function in dispersion corrected density functional theory, *J. Comput. Chem.*, 2011, **32**, 1456–1465.

32 T. H. Dunning, Gaussian basis sets for use in correlated molecular calculations. I. The atoms boron through neon and hydrogen, *J. Chem. Phys.*, 1989, **90**, 1007–1023.

33 M. J. Frisch, G. W. Trucks, H. B. Schlegel, G. E. Scuseria, M. A. Robb, J. R. Cheeseman, G. Scalmani, V. Barone, G. A. Petersson, H. Nakatsuji, X. Li, M. Caricato, A. V. Marenich, J. Bloino, B. G. Janesko, R. Gomperts, B. Mennucci, H. P. Hratchian, J. V. Ortiz, A. F. Izmaylov, J. L. Sonnenberg, D. Williams-Young, F. Ding, F. Lipparini, F. Egidi, J. Goings, B. Peng, A. Petrone, T. Henderson, D. Ranasinghe, V. G. Zakrzewski, J. Gao, N. Rega, G. Zheng, W. Liang, M. Hada, M. Ehara, K. Toyota, R. Fukuda, J. Hasegawa, M. Ishida, T. Nakajima, Y. Honda, O. Kitao, H. Nakai, T. Vreven, K. Throssell, J. A. Montgomery, Jr., J. E. Peralta, F. Ogliaro, M. J. Bearpark, J. J. Heyd, E. N. Brothers, K. N. Kudin, V. N. Staroverov, T. A. Keith, R. Kobayashi, J. Normand, K. Raghavachari, A. P. Rendell, J. C. Burant, S. S. Iyengar, J. Tomasi, M. Cossi, J. M. Millam, M. Klene, C. Adamo, R. Cammi, J. W. Ochterski, R. L. Martin, K. Morokuma, O. Farkas, J. B. Foresman and D. J. Fox, *Gaussian 16, Revision A.03*, Gaussian, Inc., Wallingford CT, 2016.

34 R. F. W. Bader, *Atoms in Molecules: A Quantum Theory; The International Series of Monographs of Chemistry*, ed. J. Halpen and M. L. H. Green, Clarendon Press, Oxford, 1990; P. L. A. Popelier, *Atoms in Molecules: An Introduction*, Prentice Hall, London, 2000.

35 T. A. Keith, *AIMAll, 19.10.12*, TK Gristmill Software, Overland Park KS, USA, 2011 Version.

36 E. R. Johnson, S. Keinan, P. Mori-Sanchez, J. Contreras-Garcia, A. J. Cohen and W. Yang, *J. Am. Chem. Soc.*, 2010, **132**, 6498–6506.

37 T. Lu and F. Chen, Multiwfn: a multifunctional wavefunction analyzer, *J. Comput. Chem.*, 2012, **33**, 580–592.

38 Jmol: an open-source Java viewer for chemical structures in 3D. http://www.jmol.org/.

39 G. A. Bain and J. F. J. Berry, *Chem. Educ.*, 2008, **85**, 532–536.

40 (*a*) R. Kannappan, S. Tanase, I. Mutikainen, U. Turpeinen and J. Reedijk, *Inorg. Chim. Acta*, 2005, **358**, 383–388; (*b*) P. R. Reddy and N. Raju, *Polyhedron*, 2012, **44**, 1–10; (*c*) C. Lochenie, S. Schlamp, A. P. Railliet, K. Robeyns, B. Weber and Y. Garcia, *CrystEngComm*, 2014, **16**, 6213.

41 H. B. F. Dixon, S. D. Clarke, G. A. Smith and T. K. Carne, *Biochem. J.*, 1991, **278**, 279–284.

42 (*a*) L. Yang, D. R. Powell and R. P. Houser, *Dalton Trans.*, 2007, 955; (*b*) A. Okuniewski, D. Rosiak, J. Chojnacki and B. Becker, *Polyhedron*, 2015, **90**, 47–57.

43 H. B. Bürgi, J. D. Dunitz, J. M. Lehn and G. Wipff, Stereochemistry of reaction paths at carbonyl centres, *Tetrahedron*, 1974, **30**, 1563–1572.

44 I. Alkorta, J. Elguero and A. Frontera, Not Only Hydrogen Bonds: Other Noncovalent Interactions, *Crystals*, 2020, **10**, 180.

45 (*a*) R. Papadakis, E. Riviére, M. Giorgi, H. Jamet, P. Rousselot-Pailley, M. Réglier, A. J. Simaan and T. Tron, *Inorg. Chem.*, 2013, **52**, 5824–5830; (*b*) E. Ruiz, A. Rodríguez-Fortea, P. Alemany and S. Alvarez, *Polyhedron*, 2001, **20**, 1323–1327; (*c*) Y. Xie, J. Ni, F. Zheng, Y. Cui, Q. Wang, S. W. Ng and W. Zhu, *Crystal Growth Des.*, 2009, **9**, 118–126.

46 (*a*) V. H. Crawford, H. W. Richardson, J. R. Wasson, D. J. Hodgson and W. E. Hatfield, *Inorg. Chem.*, 1976, **15**,

2107–2110; (*b*) M. S. Haddad, S. R. Wilson, D. J. Hodgson and D. N. Hendrickson, *J. Am. Chem. Soc.*, 1981, **103**, 384–391; (*c*) E. Ruiz, P. Alemany, S. Alvarez and J. Cano, *J. Am. Chem. Soc.*, 1997, **119**, 1297–1303; (*d*) E. Ruiz, P. Alemany, S. Alvarez and J. Cano, *Inorg. Chem.*, 1997, **36**, 3683–3688; (*e*) R. P. Doyle, M. Julve, F. Lloret, M. Nieuwenhuyzen and P. Kruger, *Dalton Trans.*, 2006, 2081–2088; (*f*) J. Sanchiz, O. Pasan, F. Fabelo, M. Lloret, C. Julve and J. Ruiz-Pérez, *Inorg. Chem.*, 2010, **49**, 7880–7889; (*g*) I. Gautier-Luneau, D. Phanon, C. Duboc, D. Luneau and J. L. Pierre, *Dalton Trans.*, 2005, 3795–3799.

47 S. Youngme, C. Chailuecha, G. A. Albada, C. Pakawatchai, N. Chaichit and J. Reedijk, *Inorg. Chim. Acta*, 2005, **358**, 1068–1078.

48 (*a*) S. S. P. Dias, V. André, J. Kłak, M. T. Duarte and A. M. Kirillov, *Cryst. Growth Des.*, 2014, **14**, 3398–3407; (*b*) E. I. Śliwa, D. S. Nesterov, J. Kłak, P. Jakimowicz, A. M. Kirillov and P. Smoleński, *Cryst. Growth Des.*, 2018, **18**, 2814–2823.

49 (*a*) B. J. Hathaway, in *Comprehensive Coordination Chemistry*, ed. G. Wilkinson, R. D. Gill and J. A. McCleverty, vol. 5, Pergamon Press, Oxford, 1987; (*b*) B. J. Hathaway and J. Chem Soc, *Dalton Trans.*, 1972, 1196–1199; (*c*) H. Elliott, B. J. Hathaway and R. C. Slade, *J. Chem. Soc. A*, 1966, 1443–1445; (*d*) I. M. Procter, B. J. Hathaway and P. Nicholls, *J. Chem. Soc. A*, 1968, 1678–1684.